

Recent trends in Sputter coating

¹B Sathvik, ²G Bharadwaj
¹Research Scholar, ²Research Scholar
 GMR INSTITUTE OF TECHNOLOGY

Abstract - Steel is an alloy of iron, carbon and other elements. Due to its high tensile strength and low cost, these are used as materials for various engineering components like tools, ships, automobiles, machines, appliances, and weaponry. There is always a high risk in the change of properties (mechanical, tribological, microstructural) when a low alloyed steel component encounters a high humidity pressure or even in an aqueous medium. So, in order to improve the surface properties hardness, wear and corrosion resistance of the steel materials various surface coating techniques are used. The sputter coating method is one of the prominent surface coating technique to improve the surface properties of the material. Present review focused on the various process parameters in sputter coating technique which are influencing the surface properties of the various types of steels. In this paper, we have presented the variation of properties with different coatings for both substrate steel and alloy steel like stainless steel and high-speed steel.

keywords - Coating, Microstructural.

I. INTRODUCTION

A coating is a thin layer that is applied to the surface of an object, usually referred to as the substrate. The purpose of applying the coating may be decorative, functional, or both. The coating may be applied all-over the object or selected areas of an object based on the requirement. An example of all of these types of coating is a product label on many drinks bottles- one side has an all-over functional coating (the adhesive) and the other side has one or more decorative coatings in an appropriate pattern (the printing) to form the words and images. Paints and lacquers are coatings that mostly have dual uses of protecting the substrate and being decorative, and the paint on large industrial pipes is presumably only for the function of preventing corrosion. Functional coatings may be applied to change the surface properties of the substrate, such as adhesion, wettability, corrosion resistance, or wear resistance. e.g., semiconductor device fabrication (where the substrate is a wafer), the coating adds a completely new property, such as a magnetic response or electrical conductivity, and forms an essential part of the finished product. Coatings may be applied as liquids, gases or solids. Hence, the coatings can be classified as,

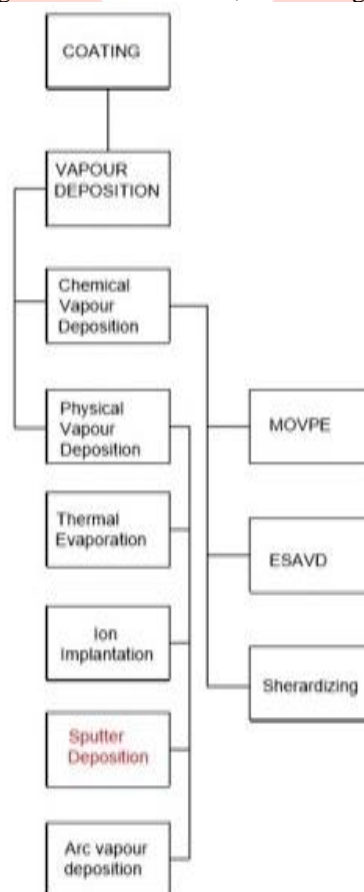


Fig.1.1 Flow chart

II. CHEMICAL VAPOR DEPOSITION

Synthetic vapor deposition (CVD) is a silt technique used to create high quality, elite, strong materials, normally under vacuum. The procedure is frequently utilized in the semiconductor industry to create thin films. In average CVD, the wafer (substrate) is presented to at least one volatile precursor, which respond or potentially break down on the substrate surface to create the desired deposit. Frequently, unpredictable side-effects are likewise delivered, which are evacuated by gas course through the response chamber. Miniaturized scale creation process broadly uses CVD to store materials in different structures including monocrystalline, polycrystalline, shapeless and epitaxial.

III. PHYSICAL VAPOR DEPOSITION

Physical vapor deposition (PVD) depicts an assortment of vacuum statement techniques which can be utilized to create thin films and coatings. PVD is portrayed by a procedure in which the material goes from a consolidated stage to a vapor stage and after that back to a thin film condensed phase. The most well-known PVD forms are sputtering and evaporation. Examples incorporate semiconductor devices, like, thin-film solar panels, aluminized PET film for packing eatables and inflatables, and titanium nitride covered cutting apparatuses for metalworking. Other than PVD tools for fabrication, special smaller tools (mainly for scientific purposes) have been developed.

IV. COMPARISON BETWEEN PHYSICAL VAPOR DEPOSITION AND CHEMICAL VAPOR DEPOSITION

One reason to use a physical vapor deposition process (such as sputtering) instead of chemical vapor deposition is the temperature requirement. CVD processes run at much higher temperatures than PVD processes, usually between 300°C and 900°C. This heat is supplied by a furnace, RF coil, or laser, but it always heats the substrate. Substrates that cannot tolerate this temperature must have thin films deposited by the physical form of vapor deposition instead. The benefit of the substrate temperature in some CVD processes is that there is less waste deposition, especially in cold-wall reactors, because only the heated surfaces are coated. With the use of a laser heating system, the chemical vapor deposition process becomes selective to the path of the laser; this is a distinct advantage over physical vapor deposition methods such as sputtering. Molecular beam epitaxy (PVD process) has a distinct advantage of atomic level control of chemical composition, film thickness, and transition sharpness. This process is relatively more expensive but is worth the added cost for applications that demand higher precision. Sputtering (PVD process) does not require the use of specialized precursor materials as used in CVD. Sputtering has a wider range of materials readily available for deposition. Another advantage of physical vapor deposition over chemical vapor deposition is the safety issue of the materials that are used for chemical vapor deposition. It is known that some precursors and some by-products are toxic, pyrophoric, or corrosive. This can cause issues with material handling and storage. There are applications that could use either deposition method successfully. However, an experienced engineer could easily recommend chemical or physical vapor deposition for a job based on criteria such as cost, film thickness, source material availability, and compositional control.

V. COMPARISON OF SPUTTER COATING WITH OTHER DEPOSITION TECHNIQUES

An important advantage of sputter deposition is that even materials with very high melting points are easily sputtered while evaporation of these materials in a resistance evaporator or Knudsen cell is problematic or impossible. Sputter deposited films have a composition close to that of the source material. The difference is due to different elements spreading differently because of their different mass (light elements are deflected more easily by the gas) but this difference is constant. Sputtered films typically have a better adhesion on the substrate than evaporated films. A target contains a large amount of material and is maintenance free making the technique suited for ultrahigh vacuum applications. Sputtering sources contain no hot parts (to avoid heating they are typically water cooled) and are compatible with reactive gases such as oxygen. Sputtering can be performed top-down while evaporation must be performed bottom-up. Advanced processes such as epitaxial growth are possible. Some disadvantages of the sputtering process are that the process is more difficult to combine with a lift-off for structuring the film. This is because the diffuse transport, characteristic of sputtering, makes a full shadow impossible. Thus, one cannot fully restrict where the atoms go, which can lead to contamination problems. Also, active control for layer-by-layer growth is difficult compared to pulsed laser deposition and inert sputtering gases are built into the growing film as impurities. Pulsed laser deposition is a variant of the sputtering deposition technique in which a laser beam is used for sputtering. Role of the sputtered and resputtered ions and the background gas is fully investigated during the pulsed laser deposition process.

VI. METHODOLOGY

Sputter deposition is a physical vapor deposition (PVD) method of a thin film deposited by sputtering. This involves emitting material from a "target" that is a source onto a "substrate" such as a silicon wafer. Re-sputtering is re-excretion of the deposited material during the deposition process by ion or atom bombardment. Sputtered atoms ejected from the target have a wide energy distribution. The sputtered ions (typically only a small fraction of the ejected particles are ionized — on the order of 1 percent) can ballistically fly from the target in straight lines and impact energetically on the substrates or vacuum chamber (causing re-sputtering). Alternatively, at higher gas pressures, the ions collide with the gas atoms that act as a moderator and move diffusively, reaching the substrates or vacuum chamber wall and condensing after undergoing a random walk. The entire range from high-energy ballistic impact to low-energy thermalized motion is accessible by changing the background gas pressure. The sputtering gas is often an inert gas such as argon.

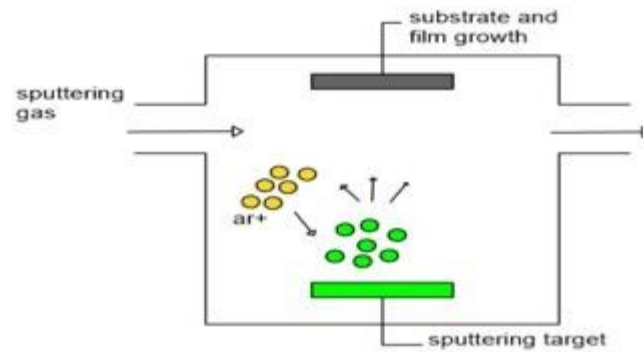


Fig.6.1.Sputter coating

VII. DISCUSSIONS

7.1 Coated with Titanium coatings

When steel was coated with TiBC, due to increasing the power ratio (c/TiB_2) from 0.25 to 1.30 the hardness, Young's modulus is decreased from 30GPa to 10GPa and 310GPa to 220GPa respectively. The progressive decrease in hardness & Young's modulus is associated with the increase in the carbon content and the formation of amorphous phases. All TiBC coatings exhibit high wear rate except the coating with a power ratio of 1.30, which exhibits lower than the non-coated steel. This behavior is associated with the crystallinity of the coatings. With the lowest power ratios, harder and more crystalline coatings are obtained, while with high power ratios the excess of carbon can precipitate and form carbon-rich phases, which act as a self-lubricating material. It is important to note that all wear rates of Ti-B-C coatings are one order of magnitude below than uncoated steel [1]. when coated with TiB₂ on nitrided AISI H13 steel, the adhesion of the TiB₂ coatings increased to ~30N after nitriding, but the hardness of the coating was lowered to 20–30 GPa. However, the adhesion of the TiB₂ coatings with a high hardness (>60 GPa) could not be improved substantially by nitriding due to the large difference in hardness between the coating and the substrate. The grain size of the TiB₂ coating was larger on the nitrided substrates, resulting in a decrease in the hardness of the coating [2]. when coated steel was coated with TiAlCN, with an increase in the C content, the structure of coatings changes from NaCl type crystalline structure to crystalline + amorphous nanocomposite structure, and then to a near amorphous structure. TiAlCN coating with optimized high hardness and low friction coefficient has been synthesized using a TiAl_{0.25}C_{0.5} target, where the maximum hardness of 2443 HV_{25g} was achieved. This coating exhibits a typical nanocomposite structure with a C content of 26.69 at.%. A significant drop in the friction coefficient of TiAlCN coating from 0.8 to 0.19 was observed when the C content reaches 26.69 at.%. Further increase of the C content in the coatings has limiting effects on further reducing the frictional coefficient [3].

when steel is coated with Titanium based coatings, the average surface roughness Ra for 0.5 hours and 1 hour on the coating was 3.946– 3.393 nm and 15.749–17.433 nm. This is due to the more deposition time that admits the formation of coarse structures which leads to an increase in surface roughness. The calculated value of hardness for the Ti–6Al–4V–2B₄C coating under 0.5 h and 1 h coating time is 7.2 GPa and 9.7 GPa respectively. The Nano hardness of the Ti–6Al–4V–2B₄C coated AISI 1040 steel substrates decreases when increasing the maximum indentation depth. The higher nano-hardness of the composite coatings is due to the finer surface morphology, more compact structure and also as a result of the homogeneous distribution of nano B₄C particles in the coating. The coefficient of friction of Ti–6Al–4V–2B₄C coated AISI 1040 steel ranges between 0.43 and 0.48 against 0.5 h coatings, 0.42 and 0.45 against 1 h coatings. The Ti–6Al–4V–2B₄C coated AISI 1040 steel exhibits specific wear rate values up to 2 times lower values than that of the uncoated AISI 1040 steel. The specific wear rate of uncoated AISI 1040 steel which produces higher specific wear rate when compared with Ti–6Al–4V–2B₄C coated AISI 1040 steel. The specific wear rate decreases as the amount of B₄C reinforcement increases for all applied normal loads but its effect is more predominant at lower loads. At 3 N loads, the specific wear rate is almost independent of the B₄C amount. It is clearly stated that this parameter brings out the development in inherent wear resistance of the coating with an increase in the amount of B₄C reinforcement. It shows that as the sliding increases, the specific wear rate of both the coatings was increased [4]. when steel is coated with TiN and TiAlN, the wear resistance of the TiN coating deposited on the hardened AISI 304 steel increased by 52.8%. The increase in the substrate's hardness by 21.1% causes the wear resistance increasing by 52.8%. The effect of wear resistance improving from the pre-hardening of a substrate by TCT and deposition of the coating is much less than the observed effect of wear resistance improving by the combination of TCT for substrate material and further deposition of vacuum coating. Increasing the hardness of the substrate by means of nitrocarburization allows diminishing to wear until the appearance of permanent deformation in the substrate material. nitrocarburization of the steel substrate enables to increase the microhardness up to 7 times, the wear resistance for working surfaces of composites by 2.3 times, and the resilience of the studied composites by more than 4.5 times. Substrate nitrocarburization substantially increases the toughness of coatings and their adhesion to the substrate, which leads to the complex enhancement of their performance characteristics including the wear and cracking resistance of the coatings [5]. when steel is coated with TiN/TiB₂, the TiN grain size increased with increasing TiN layer thickness and the change in the TiB₂ layer thickness had no significant influence on the microstructure of the TiB₂ layers. The plastic hardness of the coatings increased steadily with decreasing TiN layer thickness and with increasing TiB₂ layer thickness. The hardness increased slightly with increasing layer period. The hardness values of the multilayer coatings had a linear relationship with the TiB₂ volume fraction [6].

when steel is coated with TiB₂ by incorporation of C or MoS₂. For TiB₂-C coatings, a two-phase material is formed, consisting of diamond-like carbon and a hexagonal TiB₂ type structure into which carbon is incorporated. A friction-reducing effect was observed only at high C concentrations, above 66%, as up to this value, the DLC phase remains at less than 20% of the phase fraction. For TiB₂-MoS₂ coatings, a friction-reducing effect was observed, even at low concentrations of MoS₂. Low friction was obtained at temperatures up to 400 °C for the TiB₂-MoS₂ coatings, whilst the TiB₂-C coatings exhibited a sharp increase in friction coefficient above 150 °C, a behavior typical of graphitic coatings. At suitable compositions, a hardness approaching 20 GPa could be combined with friction coefficients as low as 0.05, as compared to 47 GPa and 0.85 for pure TiB₂ produced under comparable conditions [7]. Madaoui had observed the properties when XC48 steel is coated with TiN and TiCN, the hardness of TiCN is always higher than that of TiN. Indeed, when VSB changes from 0 to -100V, the hardness of TiCN increases from 16 GPa to a maximum of about 39 GPa. In the case of TiN, it increases from 4.9 GPa to a maximum value of 34.1 GPa and then decreases to 30 GPa. This is due to the induced microcrystalline structure in the nanocomposite coating. In the case of TiN coating, the corrosion potential is shifted to a more negative value. This is more likely due to the existence of a galvanic coupling. The reverse is observed for TiCN coating and its more positive potential could be traced back to its denser microstructure. The ratio of the corrosion rate of TiN to that of TiCN is about 200. In addition, it has been pointed out that the corrosion resistance decreases with an increasing carbon content in the coating [8]. when steel is coated with TiN/TiCN multilayer, the thick TiN/TiCN multilayer film, of which the thickness was 23.5 μm, was deposited on steel. The inner TiCN layers possessed nanocomposite structure consisting of the TiCN nanocrystalline and the amorphous carbon, and the TiN layers showed nano-columnar structure. By the scratch tests and nanoindentation, the film showed an appreciable adhesion force and a satisfactory hardness even if the thickness is 23.5 μm. Tribological test results also indicated that there was no significant change in the wear resistance of the film in contrast with other thin hard films, but the service life of the film was prolonged by the high thickness [9].

when high-speed steel is coated with TiN and influence of metallic interlayers, a thin layer of material was deposited on metal, in between the substrate and the coating. The interlayer metals chosen were W (Tungsten), Nb (Neodymium), Cr (chromium), Mo (Molybdenum), Ti (Titanium), Ag (silver), Al (Aluminum) along with these, two reference samples without interlayers were chosen they are TiNR produced using the rectangular magnetron and TiNC produced using circular magnetron. On each substrate metallic interlayer of nearly 100–150 nm. was deposited. TiN of 3.1±0.5 μm was deposited on the metallic interlayer. The circular magnetron produces 17% more hardness and modulus than rectangular magnetron during TiN coating. The hardness produced by Circular magnetron (32±4 GPa) was higher than rectangular magnetron (26±4 GPa). An elastic modulus of TiN coating is 390+/- 5 (Rectangular) and 470+/- 50 GPa (Circular). When a scratch test was done Mo and Nb show sporadic adhesion failures (failures occurring at regular intervals) remaining metals show continuously spread adhesion failures. When Rockwell hardness test was performed a certain amount of cracks can be seen on the edges of the indents TiNR, TiNC, Mo, Nb, Cr, and Ti but no spallation of the coatings. on the samples W, Ag and Al we can see coating spallation suggesting poor adhesion [10]. William had observed the properties when high-speed steel is coated with TiN, with a hardness of 24418.56 N/mm². The speed and feed were taken in such a way that uncoated drill will fail while drilling two to three holes and Coated drills can withstand up to 150 holes.

Drills are tested in two different processes.

Drill life test 1:

The uncoated dry drill makes 3.1 holes i.e 98% of the holes that TiN coated (300 holes) has made. The uncoated wet trim drill makes 6 holes but the TiN coated drill will make 300 holes, 98% more than the Uncoated drill has produced. Uncoated wet trusol makes 3 holes, TiN coated will make 10 holes. The life of the coated and uncoated drills tested in the Trim fluid was doubled over the dry cutting condition, but with the Trusol fluid, the life of the coated drill was reduced, with little difference in life for the uncoated drill in the Trusol fluid over the dry condition because of high sulfonates and amine salted.

Drill life test 2:

The sputtered coating drill has an average of 452 holes with a deviation of 96, the PVD-A has an average life of 530 holes with a deviation of 407 and that of PVD-B is 398 holes with a deviation of 209. Compared to other PVD TiN coating process reactively sputtered TiN coated drills have a smaller deviation in the number of holes cut to failure. where PVD A & B are two commercially PVD coated TiN on drills [11]. when high-speed steel is coated with TiB₂, Firstly TiB₂ coating was deposited on both stationary and rotating substrates (HSS). The deposition rate on the stationary substrate was 14 nm/min and was much higher than the rotating substrate with 8 nm/min. Deposition rate depends on the substrate-target distance, shorter the distance higher the deposition rate, and vice versa. TiB₂ coating was deposited with a different thickness of 1.4 μm and 2.5 μm on both stationary and rotating substrates. Hardness for coating with 1.4 μm was higher for stationary substrate (30.9 GPa) compared with a rotating substrate (23.6 GPa) which is 23% less than the hardness of stationary substrate. Coating with 2.5 μm was higher for stationary substrate (42.7 GPa) compared with a rotating substrate (20.4 GPa) which is 52.2% of the hardness of stationary substrate. The reduced modulus for stationary substrate was in a range of 328.1 – 368.2 GPa and that of a rotating substrate is 297.9 – 301.5 GPa. The coatings deposited on stationary substrates possess higher coating-substrate adhesion having large critical load values in a range of 527.2 - 859.6 mN but also exhibit much better resistance to plastic deformation and scratch damage as derived from the higher yield load values (976.5 - 2153.6 mN). From this we can say that coating produced on rotating substrates have low hardness and modulus values, substrate rotation has a great effect on mechanical properties [12].

when high-speed steel is coated with (Ti, Al)N layers, The (Ti, Al)N coatings were deposited by reactive a dc and Radio-frequency magnetron sputtering. It was deposited with a thickness of 1-2 μm with a Sputtering rate of rf: 1-1.5 nm/min, dc: 7-8 nm/min. Because of the change in chemical composition of nitrogen in (Ti, Al), N coatings showed color changes from metallic silver with low nitrogen contents to a very dark blue for layers with high nitrogen contents. The deposition rate of the magnetron-

sputtered (Ti, Al) N coatings decreases with increasing N₂ partial pressure this was due to the increase in nitrogen content. The hardness of the present (Ti, Al) N coatings can only be compared with microhardness values of the same coating-substrate system determined by the nitrogen flow. Values of up to 2200-2300 HV are observed at maximum intermediate flow rates. At high flow rates, a strong decrease of the hardness is found (~1750 HV). In high-rate reactive dc sputtering critical load values of up to 60 N were found for (Ti, Al) N coatings of about 1 μm thickness. Higher critical load values were found for coating with high thickness [13].

When high-speed steel is coated with TiCrAlCN/TiAlN multilayer, TiCrAlCN/TiAlN was deposited with approximately 7.2 μm thickness. It shows good metallurgical adhesion between the coating and substrate surface. The tribological tests of the TiCrAlCN/TiAlN multi-layer coatings were performed at room temperature and 150, 300, 450, and 600°C. The hardness of the multilayer coating was 23 GPa. Thickness and hardness values of the coatings increase at high target currents. At room temperature, the friction coefficient started low and then gradually increased during the test. When the test was going on, the friction coefficients for M2 HSS substrate and the coatings which were tested at RT increased with the increasing sliding distance at the end of the tests, the M2 substrate had the highest friction coefficient and the coatings which were tested at 600°C exhibited the lowest friction coefficient also shows that the sample tested at 600°C was the most stable and had the lowest friction of coefficient. All the samples have much better wear resistance than M2 substrate. The samples tested at room temperature have plastic deformation at the border. The coated sample tested at 600°C has a smaller wear scar width and depth at the temperatures and also the wear scar width and depth of the M2 substrate is much larger than the coated samples [14].

When high-speed steel is coated with TiN-NbN multilayer, four combinations of TiN/NbN coatings, with nominal thickness (in nm): 500/500, 100/10, 10/100 and 10/5, were deposited on HSS. Initially, Ti was deposited with a thickness of 10–30 nm and then TiN was deposited with a thickness of 50–250 nm. Homogeneous TiN and NbN coatings were deposited on HSS as reference material, all the above thickness should be in the range of 4–6 μm. The grain sizes were in the range of 50–55 and 20–40 nm for TiN and NbN, respectively. The 10/5 multilayer has the highest hardness. The 10/5, with approximately 33% NbN and the largest number of layers in the coating, exhibited the highest hardness (~3400 HV) as NbN has smaller grain size and in 10/5 NbN occupies very less volume compared with remaining samples [15]. In stainless steel, while coating it with TiO₂ The as-deposited surface exhibits pebble-like growth of grains with a size range of about 300–500 nm. Small voids are also present in the coating, indicating the low density of the as-deposited coating as expected at the grain boundary triple points for the coarser and granular morphologies under the sputtering conditions of low energy ion bombardment. Nitrogen in this region is dissolved in the α-Ti lattice in accordance with the TiN system where α-Ti can dissolve up to 25 at % nitrogen. After oxidation, the total thickness of the coating is larger than that of the as-deposited titanium coating (=1). The as-deposited Ti coating showed the hardness of about 1.5–3 GPa when the penetration depth was below 600 nm. After thermal oxidation at 550 °C, the surface hardness increased to above 11 GPa. When the penetration depth is below 300 nm. The friction behavior of the as-deposited coating changed suddenly at a load of around 470 mN due to adhesive failure of the coating. The average friction coefficient lower than 0.2 under unlubricated test shows the effectiveness of rutile TiO₂ coating on the stainless steel. Pitting occurs in the AISI 316 uncoated substrate at potentials above 700 mV, while no pits were formed on the oxidized coating even at potentials as high as 1000 mV. This is confirmed by morphological examination of the corroded surface by SEM [16].

While coating on stainless steel with titanium Type '316Ti' stainless steel is essentially a standard carbon 316 type with titanium stabilization. The addition of titanium reduces the risk of intercrystalline corrosion. The diffractogram of deformed austenitic stainless steels showed only phases γ and α. There was no peak indicating the presence of martensite. This was an expected result due to the stress state (quasi-static deformation), cold deformation temperature and the steel composition. In most ferrous alloys, the diffusion zone formed by nitriding cannot be seen in a metallographic image. Because the coherent precipitates are generally not large enough to resolve. For this reason, the results of the surface hardness and nitrogen profile should be carefully examined for evaluation of the diffusion layer. The nitrided layers of the deformed samples have similar morphology and appearance. Because the deformation structure and deformation-induced dislocations accelerate the growth of the nitride layer. Hardness values of all nitrided samples drop from compound layer hardness to the cold deforming hardness values due to having no diffusion layer. Thus, the low-temperature nitriding process did not eliminate the effects of the deformation hardening [17]. While coating stainless steel with TiN. TiN coatings have face-centered cubic (FCC) structure. The preferred orientation is (200) when the bias voltage is relatively low. When the bias voltage increased, the preferred orientation switched from (200) to (111) and (220), mainly favoring (111). The residual stress in the TiN coatings was measured by GIXRD. TiN (220) plane was chosen for the stress measurements in the 61–64° 2θ range. The Nano hardness and Young's modulus of the coatings were evaluated by Nanoindentation; the average value of the TiN Coatings' Young's modulus was 308.61 GPa. The maximum hardness attained was 25.5 GPa at a bias voltage of -60 V, decreasing to 20.7 GPa at -150 V. Tribofilms will hinder further abrasion of the coating. Consequently, they can lower the wear rate and prevent coating failures by inhibiting crack nucleation and propagation [18]. When high-speed steel is coated with Ti-TiN, three different combinations of Ti-TiN coatings were deposited on HSS with Ti and TiN interlayer nominal thicknesses of 0.1–1.0, 0.5–1.0 and 0.2–0.2 μm respectively. Homogeneous TiN coatings were taken as reference material. Whole thickness should not exceed 5 μm. Roughness increases with an increase in Ti content in Ti-TiN. The composite hardness and residual stress decrease with increasing amount of Ti in the Ti-TiN coating. The multilayered Ti-TiN coatings proved to have a higher fracture resistance than conventional TiN [28]. When HSS is coated with TiAlN films, the coating thicknesses of TiAlN films are in a range of 1.8–2.7 μm depending on Ti current, Al current and substrate bias. The Ti/Al ratio of TiAlN film increases with increasing substrate bias. The surface roughness of deposited TiAlN film is found to decrease with an increasing Ti fraction. The Ti/Al ratio has no effect on the growth of TiAlN films. The hardness of TiAlN films increases with increasing Al fraction, and then decreases if the Al fraction was higher than 75%. TiAlN films with 50±70% Ti fractions can exhibit a better adhesion property. The TiAlN films with a 50% Ti fraction exhibit the lowest friction coefficient (< 0.20) and it exhibits an excellent cutting performance due to the slight

adhesion of SKS-95 steel fragments during the cutting process. The TiAlN films with 44.4% Ti fraction exhibits high coefficient of friction i.e >0.50 [39].

7.2 Coated with Cr coatings

When high-speed steel is coated with CrCN, depending on Graphite target current and carbon content the coating thickness is in a range of 1.15 - 2.50 μm . When Carbon target current is 0 A, for CrN coating, the surface grains are like stones, and the grain size is about 0.2 μm . When Carbon target current is 0.3 A, the surface morphology remains unchanged, but the grain size decreases to 0.1 μm . While, when Carbon target current is 0.9 and 1.5 A there are no visible grains, which shows that the surface of the coating has been very smooth and the grain size of CrCN coatings becomes smaller and the surface becomes smoother. This helps reduce the friction coefficient and increase the hardness. Hardness increases from 1930 HV to 2300 HV i.e. hardness increases by 16%. With the increase of the carbon target current the wear ratio of the coatings decreases. For CrN coating (i.e Carbon target current is 0A), the wear ratio is $8.351 \times 10^{-15} \text{ m}^3/\text{Nm}$. For Carbon target current is 1.5 A, the wear ratio is the smallest with $3.859 \times 10^{-15} \text{ m}^3/\text{Nm}$, only 46.2% of the CrN coating [19]. when steel is coated with CrN, the surface roughness of CrN film decreases with increasing substrate temperature. The surface morphology of specimen C, which was deposited at 300 $^{\circ}\text{C}$ without bias shows a multi-faceted structure and a rather rough appearance as compared with other specimens, which was deposited at 300 $^{\circ}\text{C}$ under -290 V bias voltage. For the coatings deposited under -290 V bias, the residual stress changes from compressive to tensile state as temperature increases to 300 $^{\circ}\text{C}$. The hardness and elastic modulus values of CrN film increase with substrate temperature and bias. The hardness of the films deposited without bias is rather low as compared with those biased at the same substrate temperature. It is obvious that the increasing tendency of the hardness and elastic modulus is strongly related to the cross-sectional morphologies of films. For the thin films deposited at various temperatures and without bias voltage, two critical loads decrease with increasing substrate temperature. The adhesive failure is caused by the chipping at the edge of the scratch track [20].

When steel is coated with Al-Cr and Al-Cr-(N), the corrosion behavior of coated steels are strongly dependent on the Cr content in the Al-based coating. All Al-Cr alloy coatings are compact and dense, and thus provide improved barrier protection (for a given thickness) against the aggressive media. For a Cr content of 18 at. %, the coating also provides cathodic protection of steel, ensured by evenly distributed sacrificial dissolution of the Al-Cr coating. The cathodic protection efficiency decreases with further increasing Cr content, due to spontaneous passivation of the coating. Thus an Al-Cr coating with 18 at. % of Cr presents the best corrosion resistance in saline solution, combining an effective barrier and uniform sacrificial properties which continue to protect steel substrates in contact with the solution once open porosity develops. Nitrogen incorporation in Al-Cr coatings enhance the pitting resistance in saline solution, and for high nitrogen content, pitting corrosion is suppressed. However, this incorporation induces a potential shift towards positive values. Thus, sacrificial protection of the steel substrate is reduced. The barrier protection effect is, however conserved and perhaps enhanced since nitrogen incorporation is expected to stabilize the amorphous phase and improve coating densification [21]. when steel is coated with Cr and CrN, the hardness of the composite was twice as high as that for the steel substrate when the nitrogen content in the sputtering is 7% when a load of 0.245 N is applied. Due to the films were much harder than the substrate and the hardness increased with increasing nitrogen content in the sputtering gas. The calculated microhardness of the coatings showed that the microhardness at a 0.245 N load increased from 1229 HV at 0% N₂, to 1664 HV at 7% N₂ in the sputtering gas. This corresponds to the formation of the hard CrN phase in Cr phase as well as the solid solution strengthening of the Cr lattice by nitrogen. Since the sputter-deposited Cr and CrN films show a grain size of 7-8 nm, the hardness of Cr films is likely to be higher than that of the bulk Cr or Cr target. The critical load increases with increasing nitrogen contents in the sputtering gas. The critical loads of deposited films with 0, 3, 5 and 7% N₂ in the gas were 1.57, 5.68, 8.33 and 20.29 N₂, respectively [22].

When high-speed steel is coated with CrAlYCN/CrCN multilayer coatings were deposited with a bi-layer thickness of 2.1nm. It has a surface roughness of 0.012 μm which is extremely smooth. At a low coefficient of friction of $\mu=0.42$ and dry sliding wear coefficient of $3.5 \times 10^{-16} \text{ m}^3\text{N}^{-1}\text{m}^{-1}$ shows good tribological properties. Hardness measurements show that CrAlYCN/CrCN has Knoop hardness (HK0.025kp) value of 2735 and plastic hardness measured by nanoindentation is 39 GPa, which brings the coating close to the superhard materials for which hardness is 40 GPa. It has highly adherent coatings. CrAlYCN/CrCN coating combining high hardness ($H_p=36\text{GPa}$). In scratch adhesion tests, critical load values of $LC=55 \text{ N}$ were measured for coatings deposited on HSS [23]. when coated hss with CN_x film, with a thickness of 0.5 μm with the N₂ fraction varied from 0 to 1 and with a deposition rate of 200–600nm/h. When the films are deposited at 100 $^{\circ}\text{C}$ The friction coefficient increases from 0.19 to 0.45 with x ranging from 0 to 0.35. Frictional coefficient value increased by 58% with a change in x value and when $x=0.35$ it has a roughness of 0.3 nm. When the films are deposited at 350 $^{\circ}\text{C}$, the friction coefficient increases from 0.24 to 0.27. when $x=0.1\text{GPa}$ it shows a columnar structure, also with rough surfaces. For $x=0.25$ a high-density closely-packed granular morphology is observed and the surface is very smooth with a roughness of 0.4nm. It has a hardness of 15–20 GPa for films grown at 100 $^{\circ}\text{C}$ for all values of the gas mixture. Films were grown at 350 $^{\circ}\text{C}$ and gas mixture $>5\%$ have hardness values of 40–60 GPa i.e 60% more than film grown at 100 $^{\circ}\text{C}$ [24].

When CrSiCN coatings with a low carbon content as sliding against SiC and steel balls in water Cr element content increased slightly to 50.1 at%. Significantly, the Si element content increased gradually from 2.4 to 9.8 at%. The C element contents increased markedly from 10.5 to 17.0 at% while the content of the N element decreased rapidly from 48.5 to 22.8 at%. It was reported that the carbon atoms would replace the nitrogen atom sites as doping carbon into CrN structure the CrSiCN coating exhibited a novel Si-Si bond at 99.2 eV the thickness of CrSiCN coatings and Cr interlayer was about 1.8 μm and 0.4 μm , The maximum values of hardness and Young's modulus were 19.1 GPa and 300.8 GPa the indentation penetration depth was about 100 nm, which was less than 1/10 thickness of coatings The initial friction coefficients of CrSiCN-10, CrSiCN-20 and CrSiCN-30 were 0.25, 0.18 and 0.10 the lowest coefficient friction ($\mu=0.15$) and wear rate ($2.5 \times 10^{-7} \text{ mm}^3/\text{Nm}$) were obtained the depths of wear track on CrSiCN20 and CrSiCN-30 increased to about 0.4–0.6 μm , the wear track of CrSiCN-30 became smooth and

showed the lowest friction coefficient ($\mu=0.42$) o the highest hardness (19.1 GPa) the wore surface of CrSiCN-10 was higher than the height of substrate about 0.8 μm [25]. when high-speed steel is coated with chromium nitride, The CrN-ABS(Arc bond sputtering) films were deposited at a growth rate of 1 $\mu\text{m}\cdot\text{h}^{-1}$.The CrN-HIPIMS coating deposits films at the rate of 0.5 $\mu\text{m}\cdot\text{h}^{-1}$. 2-3 μm thick CrN or CrN/NbN was deposited.The CrN-HIPIMS coating exhibits Compressive stress values that vary over a wide range from 1.8 GPa at 75 V to 6.5 GPa at 120 V.The CrN-ABS coating exhibits relatively lower stress, ranging from 2 GPa at 75 V to 5.5 GPa at 300 V.The stress of the coating deposited at 100 V is 3 GPa.The lowest values for K_c , abrasive wear coefficient signifying the highest resistance, was observed for the CrN-HIPIMS coating $K_c= 2.2 \times 10^{-13} \text{ m}^3 \text{ N}^{-1} \text{ m}^{-1}$.The highest value of $K_c=1.8 \times 10^{-12} \text{ m}^3 \text{ N}^{-1} \text{ m}^{-1}$ was measured for the CrN-ABS coating.low-stress CrN/NbN-ABS coatings can exhibit a very high hardness(HK 0.025 = 3800).The hardness of CrN-HIPIMS was HK0.025=2800 and that of CrN - ABS was nearly HK 0.025 = 3200[27].

7.3 Other coatings

When high-speed steel is coated with NbN thin films, the growth rate of NbN_x thin films varies with N₂ partial pressure (Nitrogen partial pressure), and it is in a range of 1.3 - 4.0 $\mu\text{m}/\text{h}$. and the thickness of the film is in the range of 2.3 - 3.5 μm . This coating shows good adhesion properties with critical load values in the range of 60 - 75 N when deposited at higher PN₂ values ($\geq 3.5 \times 10^{-2} \text{ pa}$). The highest hardness, approximately 50000 N/mm² that was obtained for films deposited at lower PN₂. the lowest hardness was approximately 34000 N/mm² Obtained at higher PN₂ values. There was an increase of 32% due to the change in PN₂. Because of an increase in partial pressure grain size will increase and as a result hardness decreases. Microhardness values for NbN_x coatings measured with a UMIS-2000 ultra-micro indentation system (Berkovich indenter) are in the range of 20–45 GPa (20 000–45 000 N/mm²). The porosity value depends on nitrogen partial pressure and is in range of 0.15 - 0.6 pores / μm^2 .larger grain size for higher partial nitrogen pressure hence there will be large spaces between the grains. To know about corrosion properties in addition to different NbN samples niobium on the glass, NbN on the glass and the HSS substrate material were measured as reference materials. NbN_x coatings deposited at low and medium PN₂(1 x10⁻² – 1 x 10⁻²Pa) showed excellent corrosion behavior in 0.8 M NaCl solution [26]. when steel is coated with polyaniline(PANI), the OCP has decreased from 298 to 51 mV versus SCE initially and has started to shift in the noble direction after the 5th day of immersion. Afterward, the OCP reached a steady value of 280–290 mV versus SCE. The initial decrease of OCP may be due to the initiation of corrosion in the pin holes. The presence of polyaniline in the coating favors oxidation of the ferrous ions to stable passive iron oxide film at the pinhole region. Due to this reaction, the OCP has been shifted to noble values after 5 days of immersion. The high positive values of OCP indicate the formation of a protective passive film on iron. The resistance value of the coating (R_c) is decreased initially from 520 to 220 $\text{k}\Omega\text{cm}^2$ after 3 days of immersion and then increased gradually to 690 $\text{k}\Omega\text{cm}^2$ after 28 days of immersion. This shows the increased protective property of the coating. The capacitance values of the coating (C_c) are decreased from 1.7 to 0.22 nF/cm² indicating the protective property of the coating. This is due to the conducting nature of the coating, the oxygen reduction reaction takes place on the coating, while the oxidation of ferrous ions to iron oxides takes place on the exposed iron surface at pinhole areas and under the film in neutral media [29].

When ZrN/ZrO₂ multilayer coatings deposited on 304 stainless steel using multi-arc ion plating The thickness of the ZrN single layer coating is about 4.8 μm The surface elemental composition was obtained from XPS analysis: Zr-46.2 at%, N-21.9 at% and O-31.9 at%. Results confirmed that there is an oxide top-layer covered on the surface of ZrN coating due to the reactive nature of ZrN and surface adsorption The bilayer coating is formed by 3.2 μm thick ZrN and 3.8 μm thick ZrO₂ the elemental composition of ZrO₂ layer obtained from XPS analysis is: Zr-32.1 at% and O-67.9 at%. SEM analysis of film thickness confirmed that the deposition rates of both the ZrN and ZrO₂ sub-layers were ~80 nm/min. the chamber temperature was increased slowly from 300 °Cto 350 °Cfor the unremitting thermal radiation from the target surface, whereas it was kept at 300 °Cduring the multilayer coating deposition process. the ZrO₂ exhibits a good corrosion resistance in the 3.5 wt% NaCl solution. the bilayer sample was rapidly increased to the similar value of the 304 SS at 0.02 V, indicating that the corrosive medium reached the surface of the substrate during the corrosion tests. This proves that the ZrO₂ layer is fragile with large stress [30]. when Plasma nitriding of 316L stainless steel in two different N₂-H₂ atmospheres The nitrided layers of HN and LN are composed of two layers; in the case of HN, the uppermost is about 15 μm and the bottom one, ~ 4 μm . In the case of LN, the uppermost is ~14 μm and the bottom one, ~ 2.5 μm thick. HN shows a higher concentration of nitrogen and the total nitrided layer is about 20 μm thick; whereas LN has lower nitrogen content, a larger gradient and the total nitrided layer extends to approximately 15 μm The surface hardness after the nitriding treatments in HN and LN samples, increased from 170 HV. The current density of HN and LN is greater than the UN, although LN has a current density 30 times lower than HN at 2.5 V Carbon is contaminant coming from the reactor walls, and it is pushed back by N ions, this phenomenon is called "sweeping" [31].

When Thermal stability, wettability, and corrosion resistance of sputtered ceria films on 316 stainless steel the RMS roughness decreased from 7.32 nm to 4.87 nm the RMS roughness increased significantly to a high value of 23.7 nm. it has been found that more oxygen vacancies are formed under high oxygen flow conditions The samples annealed at 400 °C and 700 °C displayed hydrophobic behaviors after 14-day exposure in air, the water contact angles were 98.3°c and 99.8°c. all annealed samples exhibited different degrees of wettability after the annealing treatments and the 1000 °C annealing surface was still hydrophilic with contact angle ~67.4°c. The results suggest that surface hydrocarbon contamination is not sufficient to explain the hydrophobic behavior of ceria films. the polarization curves of ceria samples shifted towards higher potentials and exhibited much smaller current densities except for the film annealed at 1000 °C, indicating the effective corrosion protection of ceria films. As-deposited film and 700 °C annealing sample both exhibited a two-regime anodic polarization behavior The abrupt increase in the anodic curves for the as-deposited film and 700 °C annealing sample suggested that the Ce/ceria system deteriorated with immersion time and gradually showed the galvanic effect. The best anti-corrosion behavior was observed for the film annealed at 400 °C. the film annealed at 400 °C provided the best corrosion protection for 316 SS [32].

When DC magnetron sputtered Mo-based coatings on hard-chrome plated AISI 316 stainless steel In the case of MoCN, MoCN-HC displays only MoN phase with distinctive two equally pronounced peaks at 36.1 and 41.9° while MoCN-UHC exhibits considerably broader MoN peaks with an additional overlapped peak at 40.4°. In contrast, MoC-HC shows broad and low Mo₂C peaks while MoC-UHC displays sharp MoC and Mo₂C contributions. These results indicate that molybdenum carbide phases are better formed on stainless steel than hard chrome substrates. the sputtered MoN is the best for surface smoothing while MoCN and MoC provide inferior improvements of roughness on Stainless-HC and Stainless-UHC surfaces. It is seen that the hardness value of the Stainless-HC (~6.3 GPa) is considerably higher than that of stainless steel (~4.2 GPa) and the values agree well with their standard values. With Mo-based coatings, the hardness values of Stainless-UHC and Stainless-HC groups increase substantially and the MoN coating exhibits the highest hardest while the MoCN coating shows the lowest hardness among all Mo-based coatings the measured Hs values of 3.95 and 6.08 GPa for Stainless-HC and Stainless-UHC The results of one-way ANOVA confirmed that there are statistically significant variations in the wear rates among samples with different coating materials at the confidence interval of 95% The increase of oxygen content indicates the oxidation of stainless steel during the dry abrasion process, which naturally generates heat leading to a high surface temperature and oxidative wear mechanism [33].

When Sputtered MnCu metallic coating on ferritic stainless steel. The MnCu coating with a thickness of around 5 µm. oxidation kinetics of the samples in air at 800 C. The high mass gain of the coated bare steel should be caused by the oxidation of both MnCu coating and steel substrate The scale is about 7 mm thick in the area without spallation, indicating the increase in thickness of scale has caused serious spallation non-penetrative and closed pores in the scale are observable, which should be caused by the outward diffusion of metal ions in the MnCu coating during thermal exposure. the pre-oxidized steel with MnCu coating that more pores result in the slightly localized spallation of the surface scale the phase structure of the oxide scale formed on the bare and pre-oxidized steel samples with MnCu coatings after oxidation in air at 800 C. the inner Cr-rich layer should exist as a thin Cr₂O₃ layer with (Mn, Cr)₃O₄ spinel. In the case of the pre-oxidized steel with MnCu coating, the surface scale mainly consists of (Mn, Cu)₃O₄ spinel and CuO. MnCu coatings are much lower than 31.1 mΩ cm², the oxide scale formed on the bare steel with MnCu coating is mainly composed of an outer layer of (Mn, Cu)₃O₄ spinel with Fe and an inner layer of Cr₂O₃/(Mn, Cr)₃O₄ after oxidation in air at 800 C [34]. when Stainless steel coatings sputter-deposited on tungsten carbide powder particles, to determine the adhesion of the coating a scratch test was performed in the stainless steel coating (700 W, 1 h) deposited on WC-Co substrates, under loads from 50 up to 200 N to evaluate the pressing behavior, the coated powders were uniaxially pressed in the range 60–250 MPa, resulting in pressed compacts with 10 mm in diameter and approximately 3 mm thick. The firing cycle involved a heating rate of 5 8C min up to a maximum temperature of y1 1325 8C The powder particles were uniformly coated, which results in a high chemical homogeneity in the distribution of powder constituents This observation strengthens the interest of the use of coated powders, because the exclusion of the pressing lubricant leads to the removal of two stages of the conventional WC based cemented carbides processing, Addition of binder by this sputtering technique is shown to be very effective in promoting densification, which may also be attributed to the high degree of uniformity in binder distribution and to the high reactivity of the binder phase[35].

When PVD sputtered coatings on the corrosion resistance of AISI 304 stainless steel coating thickness of 2.5 mm and surface roughness (Ra value) of 0.15~0.21 mm. DLC film exhibited the highest hardness of 3810 HV, followed by TiCN at 2470 HV, and then CrN at 1738 HV. the DLC coated sample has the lowest corrosion weight loss and the lowest corrosion rate The corrosion rate of a un-coated specimen was about ten times faster than DLC coated, and two times faster than TiCN or CrN coated PVD coatings were again proved to be useful against resisting corrosion in the corrosion media. DLC film still played the best role, CrN film next and then TiCN film. It was noticeable that the CrN film initially seemed to be very effective for corrosion resistance In H₂SO₄ solution, DLC film still produced the best corrosion resistance and within 100 h immersion time [36]. when coatings of 10-15µm thick are deposited below 200 °C on well-prepared and negatively biased (- 100 V) steel substrates. The total pressure of deposition in the Ar-N₂ gas mixture lies between 0.4 and 4 Pa. a laboratory sputtering plant (LSP) with a chamber volume of 0.03 m³ and an industrial sputtering prototype (ISP) whose chamber volume is 0.04 m³. A low total deposition pressure of 0.4 Pa. A substrate temperature T_s~300°C is obtained in the LSP by means of an additional heating stage nitrogen concentration is higher than 25 at.%N. This avoids the formation of quasi0921-5093/91/\$3.50 © Elsevier Sequoia/Printed in The Netherlands amorphous as-sputtered deposits and allows unambiguous crystalline structures to develop. Nitrogen diffusion layers with a thickness of about 5µm are obtained by plasma nitriding, below 400 °C. The argon concentration is less than 0.3 at.%. With Ar-N₂ gas mixtures containing up to 50vol.%N₂ the highest nitrogen concentration of the deposits is about 42 at.%. Higher nitrogen concentrations can be achieved in the coatings by sputtering in pure nitrogen at a total pressure of 4 Pa The microhardness starts from 7000 MPa, increases with the nitrogen concentration up to 15000 MPa and then slightly decreases and stabilizes at about 12 000 MPa. The nitrogen concentration in the inner region of the layer lies between 24 at.% N. the nitriding of a 316L stainless steel sample at 400 °C during 60 h leads to a YN diffusion layer 10 pm thick whose nitrogen surface concentration is 24 at.% N[37].

When DLC coatings were deposited on untreated and plasma nitride (at 400 °C, 500 °C and 600 °C for 1 h and 4 h) AISI 4140 steel substrates, the hardness and residual stress values of plasma nitride samples and DLC coatings deposited on plasma nitride samples increased with increasing plasma nitriding temperature and time. The plasma nitride samples at 600 °C for 4 h process time exhibited the highest surface hardness (1750–1800 HV0.01) and residual stress values. The friction coefficient values of samples decreased under vacuum conditions. Also, the friction coefficient values of plasma nitride and duplex treatment samples decreased with increasing plasma nitriding temperature and process time under both conditions. The two factors, increasing surface roughness and hard adhesive particles, cause to increases the friction coefficient values. On the other hand, DLC coating leads to decrease friction due to the formation of such transfer layers on sliding-ball surfaces. All treatments

reduced the wear rate of the material in comparison to the untreated substrate in parallel with friction coefficients. Plasma nitriding treatments, DLC coating, and duplex treatments significantly increased the surface hardness of untreated substrate [38].

When steel is coated with WC, films deposited from 17 and 24% CH₄ gas mixtures showed the highest hardness: 24 and 26 GPa, largely superseding the W layer hardness. The hardened steel substrate did not change its hardness value (9 GPa) before and after coating deposition. In the lower load range, both samples showed a very low friction coefficient. Beyond a threshold load, the friction coefficient increases due to the onset of cohesive failure of the coatings. An abrupt change of friction coefficient appears at the critical load, L_c, due to the adhesive C failure of the coatings. The WC overlayer provides a great reduction of the wear rate under dry sliding. A range of coating compositions and mechanical behaviors can be obtained by varying the methane concentration in the sputtering gas [39]. when hss is coated with MoS₂, Addition of titanium to the MoS₂ coating results in hardness values of over 400 HV. The coating was also deposited onto forming dies, punches, taps, and gears for testing. Most coating survives for 10 000 cycles under the reciprocating test at 100 N load. A coated drill did not show any failures after 938 holes at 6000 rpm and 720 holes at 7000 rpm when the tests were stopped. The coated dies gave 800000 coins, more than double the number of coins the standard Cr-plated punch (375000), and uncoated punch (200000) was producing at the end of testing [40].

7.4 Applications Of Sputter Coating

There are various applications of sputter coating in modern technology they are in aerospace and defense we can use sputtering in heads-up cockpit displays, jet turbine engines, a mirror for optical and x-ray telescopes, night vision equipment. And also used in Anti-corrosion coatings, Anti-seize coatings, dies and molds, sewing needles, tools and drill bit hardening. These are often used in automotive industries mainly in auto headlights and taillights, auto trim components, drive train bearings and components, wheels and rims. In the medical field to sputtering plays a vital role that is in Angioplasty devices, anti-rejection coatings, radiation capsules, a dental implant. In the Security field, they are mainly used in markings and holograms for currency, one-way security windows. while coming to electronics sputtering is used in Flip-chip backside metallization, Gate dielectric, an inter-layer dielectric, on-chip interconnects and inter-level bias, passive thin film components, printed circuit boards, sensors, surface acoustic wave(SAW) devices. Apart from these, sputtering is also used in decorative purposes such as in building glass, building hardware, clothing, jewelry, packaging, plumbing fixtures, toys etc.

VIII. CONCLUSION

In this paper, we had studied various coatings on various steels and its alloys. Mainly, the properties of steels like mechanical, chemical and tribological are increased when the steel is coated with hard coatings like Titanium and various metals incorporated in Titanium. The other multilayer coatings have shown a significant improvement in properties but they are less significant compared to titanium coatings. Nitrocarbization before coating with titanium coatings will increase the microhardness to 7 times than the steel. On the other hand, the properties of stainless steel will increase when coated with Molybdenum alloys. The surface roughness of the stainless steel will decrease when compared to other hard chrome substrates which result in less wear resistance. Because of sputter coating on high-speed steel hardness of the substance increases depending on the thickness of the coating. Coating thickness depends on the distance between the magnetron and the substance. Generally, the wear rate decrease with sputter coating. With the use of interlayer in between the substrate and coating the hardness increases. The adhesion properties may vary depending on interlayer material.

REFERENCES

- [1] Contreras, "Microstructure, mechanical and tribological properties of TiBC coatings by DC magnetron sputtering onto AISI M2 steel using independent TiB₂ and graphite targets".
- [2] Bohwan Park, "Adhesion properties of TiB₂ coatings on nitrided AISI H13 steel".
- [3] Xuhai Zhang, "Effect of carbon on TiAlCN coatings deposited by reactive magnetron sputtering".
- [4] Selvakumar, "Microstructure, surface topography and sliding wear behaviour of titanium based coating on AISI 1040 steel by magnetron sputtering".
- [5] Komarov, "The effect of steel substrate pre-hardening on structural, mechanical, and tribological properties of magnetron sputtered TiN and TiAlN coatings".
- [6] Ju-Wan Lim, "Mechanical properties of TiNyTiB multilayers deposited by plasma enhanced chemical vapor deposition".
- [7] Gilmore, "Preparation and characterisation of low-friction TiB₂ -based coatings by incorporation of C or MoS₂".
- [8] Madaoui, "Structural, mechanical and electrochemical comparison of TiN and TiCN coatings on XC48 steel substrates in NaCl 3.5% water solution".
- [9] Jianyun Zheng, "A thick TiN/TiCN multilayer film by DC magnetron sputtering".
- [10] Gerth, "The influence of metallic interlayers on the adhesion of PVD TiN coatings on high-speed steel".
- [11] William D Sproul, "High Rate Reactively Sputtered Tin Coatings On High Speed Steel Drills".
- [12] Panich, "Effect of substrate rotation on structure, hardness and adhesion of magnetron sputtered TiB₂ coating on high speed steel".
- [13] Jehn, "Morphology and properties of sputtered (Ti,Al)N layers on high speed steel substrates as a function of deposition temperature and sputtering atmosphere".
- [14] Sukuroglu, "Investigation of high temperature wear resistance of TiCrAlCN/TiAlN multilayer coatings over M2 steel".
- [15] Mats Larsson, "Deposition and microstructure of PVD TiN-NbN multilayered coatings by combined reactive electron beam evaporation and DC sputtering".

- [16] D. Siva Rama Krishna, "Thermally oxidised rutile-TiO₂ coating on stainless steel for tribological properties and corrosion resistance enhancement".
- [17] Fatih Kahraman, "Low Temperature Nitriding Behavior of Compressive Deformed AISI 316Ti Austenitic Stainless Steels".
- [18] Yeting Xi, "Residual stress and microstructure effects on mechanical, tribological and electrical properties of TiN coatings on 304 stainless steel".
- [19] Pengfei, "Study on tribological property of CrCN coating based on magnetron sputtering plating technique".
- [20] Jyh-Wei Lee, "The mechanical properties evaluation of the CrN coatings deposited by the pulsed DC reactive magnetron sputtering".
- [21] Creus, "Corrosion behaviour of amorphous Al-Cr and Al-Cr-(N) coatings deposited by dc magnetron sputtering on mild steel substrate".
- [22] J.W.Seok, "Sputter-deposited nanocrystalline Cr and CrN coatings on steels".
- [23] Hovsepiyan, "Comparison of microstructure and mechanical properties of chromium nitride-based coatings deposited by high power impulse magnetron sputtering and by the combined steered cathodic arc/unbalanced magnetron technique".
- [24] Broitman, "Mechanical and tribological properties of CN_x films deposited by reactive magnetron sputtering".
- [25] Zhiwei Wu, "Friction and wear properties of CrSiCN coatings with low carbon content as sliding against SiC and steel balls in water".
- [26] Fenker, "Deposition of NbN thin films onto high-speed steel using reactive magnetron sputtering for corrosion protective applications".
- [27] Ehiasarian, "Comparison of microstructure and mechanical properties of chromium nitride-based coatings deposited by high power impulse magnetron sputtering and by the combined steered cathodic arc/unbalanced magnetron technique".
- [28] Mats Larsson, "Deposition and mechanical properties of multilayered PVD Ti-TiN coatings".
- [29] S. Sathiyarayanan, "Corrosion protection of steel by polyaniline (PANI) pigmented paint coatings".
- [30] Zhefeng Le, "Corrosion performance of ZrN/ZrO₂ multilayer coatings deposited on 304 stainless steel using multi-arc ion plating".
- [31] Evangelina De Las Heras, "Plasma nitriding of 316L stainless steel in two different N₂-H₂ atmospheres - Influence on microstructure and corrosion resistance".
- [32] Zhen Shi, "Thermal stability, wettability and corrosion resistance of sputtered ceria films on 316 stainless steel".
- [33] Parinya Srisattayakul, "Reciprocating two-body abrasive wear behavior of DC magnetron sputtered Mo-based coatings on hard-chrome plated AISI 316 stainless steel".
- [34] Shujiang Geng, "Sputtered MnCu metallic coating on ferritic stainless steel for solid oxide fuel cell interconnects application".
- [35] C.M. Fernandes, "Stainless steel coatings sputter-deposited on tungsten carbide powder particles".
- [36] Hui-Ping Feng, "Effects of PVD sputtered coatings on the corrosion resistance of AISI 304 stainless steel".
- [37] A.Saker, "Properties of sputtered stainless steel-nitrogen coatings and structural analogy with low temperature plasma nitrided layers of austenitic steels".
- [38] Kovacia, " friction and wear performance of DLC coatings deposited on plasma nitrided AISI 4140 steel by magnetron sputtering under air and vacuum conditions".
- [39] Esteve, "Mechanical and tribological properties of tungsten carbide sputtered coatings".
- [40] Teer, "The tribological properties of MoS₂/metal composite coatings deposited by closed field magnetron sputtering".
- [41] S.K. Wu, "An investigation of unbalanced-magnetron sputtered TiAlN Films on SKH51 high-speed steel".
- [42] F.B. Pickering, Proceedings of Stainless Steels '84, Goteberg, Sweden, 1984.